Synthesis and Characterization of Water-Soluble and Bifunctional ZnO−Au Nanocomposites

Xin Wang,[†] Xianggui Kong,*[,†] Yi Yu,[†] and Hong Zhang*[,‡]

Key Laboratory of Excited State Processes, Changchun Institute of Optics Fine Mechanics and Physics, Chinese Academy of Sciences, Changchun 130033, People's Republic of China, and Van't Hoff Institute for Molecular Science, Universiteit van Amsterdam, Nieuwe Achtergracht 166, 1018 WV Amsterdam, The Netherlands

The ability to synthesize multicomponent nanocomposites (NCs) is important for exploring their functional properties of not only individual single components but also their combinations in technological applications. This paper presents an investigation on the synthesis and characterization of water-soluble and bifunctional ZnO−Au NCs, of which ZnO provides fluorescence and Au is used for organic functionality for bioconjugation. ZnO nanocrystals were employed as seeding material for nucleation and growth of reduced gold by citrate to form the water-soluble ZnO−Au NCs. The morphology and components of the ZnO−Au NCs, characterized by the TEM and XRD, respectively, demonstrate a dumbbell-like shape and crystalline wurtzite ZnO together with face-center-cubic Au nanoparticles. The surface plasmon absorption band of ZnO−Au NCs in aqueous solution is distinctly broadened and red-shifted relative to monometallic Au nanoparticles, and the UV emission intensity is higher by about 1 order of magnitude in ZnO−Au NCs than in pure ZnO nanocrystals; these observations reflect the strong interfacial interaction between ZnO and Au. Moreover, multiphonon Raman scattering of ZnO is also largely enhanced by the strongly localized electromagnetic field of the Au surface plasmon.

Introduction

Over the past several years, colloidal semiconductor nanocrystals have attracted considerable attention owing to their unique size-dependent optical and electronic properties, based on the quantum confinement effect of the electronic states. Most research has focused on optical, electronic, optoelectronic, and magnetic properties and corresponding technology applications, such as light-emitting diodes (LED), optical data storage devices, sensors, and microlasers.[1−3] Lately, a new direction has emerged in potential biotechnological applications such as luminescence tagging, immunoassay, drug delivery, and cellular imaging.[4−7] Especially, fluorescent semiconductor nanocrystals (such as CdSe, CdTe, CdS), as a new type of biolabel, have advantages over conventional chemical fluorophores and visible fluorescent proteins in photostability and sensitivity as well as in other aspects.[7] As a fluorescent semiconductor material, ZnO nanocrystals exhibit much higher chemical stability and safety relative to the toxic Cd element semiconductor nanocrystals. Thus, fluorescent ZnO nanocrystals have become a biofriendly candidate for biological technology applications.[8]

Generally, the synthesis of high-quality ZnO nanocrystals is performed in organic media. However, water-solubility and biocompatibility of ZnO nanocrystals remain a challenge to researchers, which are primary prerequisites for their biological application. Surface modification to resolve the non-biocompatibility of inorganic materials was usually realized by functionalization with water-soluble ligands, silanization, and en-

capsulation within block-copolymer micelles.[9,10] Although these surface modifications brought little or no improvement of the electronic, optical, and magnetic functionality of the nanocrystals, a complicated chemical synthesis could not be avoided in these processes. As is well-known, nanosized gold possesses many excellent properties, such as easy reductive preparation, water-solubility, high chemical stability, and significant biocompatibility and affinity.[11] Moreover, it has also been well-established that efficiently functional amine/thiol terminal groups are able to bind stably to the gold surface for conjugation with bioactive molecules such as antibody, nucleic acid, peptides, protein, and DNA.[11,12] The prospect of developing new multifunctional nanocomposites (NCs) of metal gold hybridized with inorganic components boosts relevant research.[13−22] The advanced functionalities appear only in the hybridized heterostructure composites but not in their individual single-component counterparts. In the case of multifunctional Au composites, examples include Fe/Au,[12] Fe-oxide/Au,[14,15] Fe_3O_4−Au,[16,17] Ag/Au,[18] CdSe−Au,[19,20] Cu_2S/Au,[21] PbSe−Au−Fe_3O_4,[22] etc.

In our efforts to develop multifunctional NCs with solubility and biocompatibility in aqueous solution, we have recently demonstrated a significant strategy of biocompatible Au growing on the surface of seeding ZnO to form water-soluble ZnO−Au NCs in which the ZnO and Au components are combined to provide fluorescence and further organic functionality for bioconjugation. The dumbbell-shaped ZnO−Au NCs are formed through nucleation and growth of reduced Au at suitable sites on the ZnO surface. The structural and optical properties are studied in detail by XRD, TEM, and spectroscopy, such as UV−vis absorption, photoluminescence (PL), and Raman scattering. The investigation on the functional multicomponent composites is motivated not only by their application in biology but also

---

* To whom correspondence should be addressed. Tel: +86-431-6176313; fax: +86-431-4627031; e-mail: xgkong14@ciomp.ac.cn; h.zhang@uva.nl.
† Chinese Academy of Sciences.
‡ Universiteit van Amsterdam.

Water-Soluble and Bifunctional ZnO−Au Nanocomposites

J. Phys. Chem. C, Vol. 111, No. 10, 2007 **3837**

by the fundamental interest to better understand the physical mechanism of interfacial interaction of metal Au and semiconductor ZnO components.

Experimental Section

Preparation of ZnO Nanocolloids. A ZnO nanocolloidal suspension was prepared following, with minor modification, the method described by Anderson.[23] Briefly, an amount of 50 mL ethanol containing 1.10 g zinc acetate dihydrate (98[+]%, Beijing Chemical) was refluxed while stirring at about 80 °C for 180 min. After this procedure, a clear precursor solution was obtained followed by gradual cooling to room temperature under a nitrogen atmosphere (to prevent ambient moisture). The precursor was hydrolyzed by adding 0.29 g lithium hydroxide monohydrate power (from Fluka) in an ultrasonic bath at 0 °C for 20 min. Through a 0.1 μm glass fiber filter the ZnO colloid suspension became transparent.

Preparation of Water-Soluble ZnO−Au NCs. To realize water-soluble and stable ZnO−Au NCs, a general and simple aqueous-based synthesis was introduced in this paper. The as-prepared ZnO suspension in ethanol (6.0 mL) was precipitated by adding a very dilute trisodium citrate aqueous solution, and the obtained precipitate by centrifugation was washed with the trisodium citrate solution several times. For preparation of ZnO−Au NCs, the washed ZnO nanocrystals were redispersed in a 30 mL stock solution of trisodium citrate (3.0 mM) with the aid of ultrasonic irradiation, and then 20 mL aq 0.5 mM HAuCl₄ solution was added while vigorously stirring at room temperature. During vigorous stirring for at least 48 h, these hydrophobic ZnO nanocrystals were converted into water-soluble ZnO−Au NCs, followed by a color-change from pale yellow to deep pink. These ZnO−Au nanocomposites homogeneously dispersed in aqueous solution are able to remain stable for half a year or even longer. For comparison, monometallic gold nanoparticles in the absence of ZnO were also prepared via the same method of citrate reduction in dilute HAuCl₄ aqueous solution at about the boiling point of water following the known method.[24,25]

Characterizations of ZnO−Au NCs. The crystal structure and phase identification of the NCs were determined from the X-ray diffraction patterns recorded on a Bruker D8 Advanced diffractometer using monochromatized Cu Kα radiation (λ = 1.5418 Å). The morphology and size of the NCs were determined utilizing transmission electron microscopy (TEM, Hitachi H-8100IV, 200 kV) at a magnification factor of 200 000×. The high-resolution TEM images were acquired using a JEOL JEM-3010 (acceleration voltage of 300 kV). TEM samples were prepared by placing one drop of the suspended nanocomposite solution onto a carbon-coated copper grid and allowing it to dry in air. The UV−visible optical absorption and photoluminescence spectra were recorded on Shimadzu UV-3103PC and Hitachi F4500 spectrophotometers, respectively, using a 1 cm light path quartz cuvette. The resonant Raman spectra were measured on a Jobin-Yvon LabRam Raman microspectrometer system equipped with 1800 grooves/mm holographic gratings in the backscattering configuration under the excitation of a 325 nm line out of a 20 mW He−Cd laser.

Results and Discussion

Synthesis of ZnO−Au NCs. An aqueous-based synthetic method is utilized to produce heterostructure NCs under ambient conditions. The formation of water-soluble ZnO−Au NCs is based on nucleation and growth of reduced Au by citrate on the selective and suitable surface sites of ZnO that could serve

SCHEME 1: Schematic Illustration of the Formation of ZnO−Au NCs
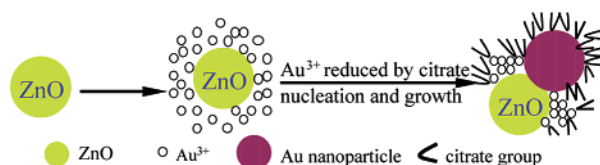
as seeds for the formation of heterogeneous nanostructure composites. The precipitated ZnO nanocrystals were redispersed in trisodium citrate aqueous solution and were mixed by adding HAuCl₄ solution during vigorous stirring at room temperature. This turbid mixture solution became gradually clear and eventually deep pink after 48 h, which indicated the formation of Au nanoparticles. The synthetic mechanism of ZnO−Au NCs is proposed and illustrated in Scheme 1, which comprises three major steps and starts with ZnO seed formation. In detail, first, gold precursor locates selectively at suitable sites on the surface of ZnO seeds surrounded with citrate groups. Subsequently, those sites on the ZnO surface act as centers for the reduction of Au^{3+} by citrate and then form nucleation sites for reduced Au atoms. Finally, reduction of Au^{3+} occurs at the preexisting nucleation sites followed by nucleation and growth of reduced Au atoms or nanoclusters. Note that the nucleation and growth of Au nanoparticles are performed at room temperature, different from the previous reported process that occurs at water-boiling temperature.[24] In the control experiment, no reaction was observed in the absence of ZnO in the solution mixture. This unambiguously reveals that ZnO nanocrystals redispersed in the trisodium citrate solution play an important role in the room temperature reduction of the Au precursor by citrate. The reaction at room temperature requires a long growth time, suppressing rapid nucleation of monometallic Au nanoparticles that are unassociated with the ZnO nanocrystals. In recent studies, Xu et al.[18] have reported the formation of Ag heterodimer nanoparticles by Fe₃O₄ or Au acting as catalyst for the reduction of Ag$^+$ and self-catalyzed reduction of Ag$^+$. Similarly, ZnO nanocrystals in the solution mixture can also promote the reduction of Au^{3+} by citrate to Au atoms or nanoclusters. In the above process, nonepitaxial nucleation and growth of Au are realized on the ZnO-seed surface without additional binding chemical agents, resulting in a dumbbell-shape heterogeneous nanostructure instead of a core−shell nanostructure because of the lattice mismatch between ZnO and Au. The obtained ZnO−Au NCs still remain stably dispersed in the aqueous media for more than 6 months (Figure 4A). In the trisodium citrate solution (pH = 8.0) ZnO nanoparticles are positively charged because the PZC (point of zero charge) of ZnO is 11,[26] and the negatively charged Au nanoparticles are attached to the ZnO nanocrystals through electrostatic affinity, which probably enables the citrate-stabilized ZnO−Au NCs to be stable in aqueous solution. Recently, there have been reports on two or more distinct composition heterostructures with a large lattice mismatch, such as Fe₃O₄ (Fe or Fe₂O₃)/Au,[12−17] (Fe₃O₄)/Ag,[18] PbSe−Au−Fe₃O₄,[22] Co/CdSe,[27] γ-Fe₂O₃/CdS,[28] and FePt/Ag(CdS),[29] whereas their formation mechanism remains to be further elucidated.

Previous attempts to form nanostructure composites containing an Au component were based on the aminosilane-coated nanoparticle surface (Fe oxide and SiO₂) acting as an attachment point for small colloidal Au through chemical binding affinity.[15,30−32] Growth of these attached gold nanoparticles was then performed to achieve the formation of Au-containing NCs following the subsequent reduction of Au^{3+} by the reducing
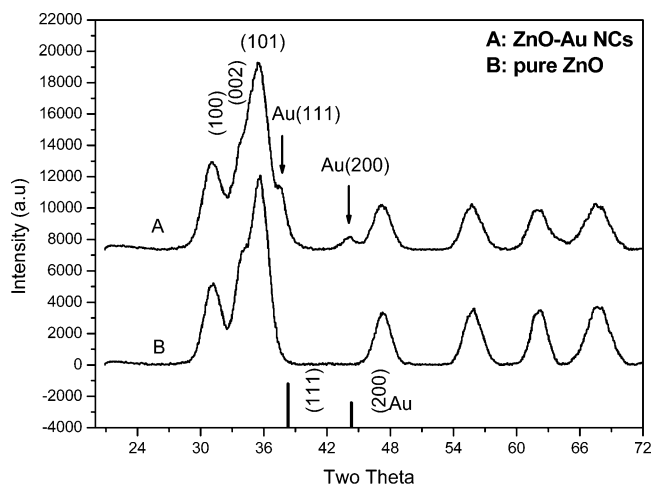
Figure 1. XRD patterns of (A) ZnO−Au NCs and (B) pure ZnO nanocrystals. Two additional diffraction peaks (marked with arrow) corresponding to face-center-cubic structure Au nanoparticles. (Two main diffraction peaks of bulk gold shown in solid line at the bottom.)

agent. However, in the synthesis of ZnO−Au NCs no binding agents were employed to bind the Au precursor on the surface of ZnO for the growth of Au nanoparticles, and therefore gold nanoparticles, as well as Ag heterodimer nanoparticles,[18] can also directly nucleate and grow on the metal or metal oxide nanoparticle surface without chemical binding agents.[13]

Structure and Morphology of ZnO−Au NCs. The structure, crystalline phase, size, and morphology of ZnO−Au NCs were determined by power X-ray diffraction (XRD) and transmission electron microscopy (TEM). The well-resolved XRD patterns of the final ZnO−Au NC samples are displayed in Figure 1A, where two additional diffraction peaks (as marked with arrow) appear compared to pure hexagonal-wurtzite ZnO nanocrystals (Figure 1B). The two additional peaks at $2\theta = 38.33$ and $44.21°$ are assigned to the diffraction lines of (111) and (200) planes of the face-center-cubic (fcc) gold, respectively. Their position and relative intensities are in agreement with the JCPDS (No. 65-2870) of bulk gold, which further proves the formation of crystalline Au. The crystalline domain sizes, estimated from the broadening of X-ray diffraction peaks according to the Scherrer equation, are about 4.3 and 6.8 nm for ZnO and Au nanoparticles, respectively.

Representative low-magnification TEM images of the ZnO−Au NCs are illustrated in Figure 2A, where the measured average diameter is 4.9 and 7.1 nm for ZnO and Au, respectively, consistent with the above X-ray results. As shown in the image, the ZnO−Au NCs are fairly monodispersive, and their shapes are different from the spherical ZnO nanoparticles
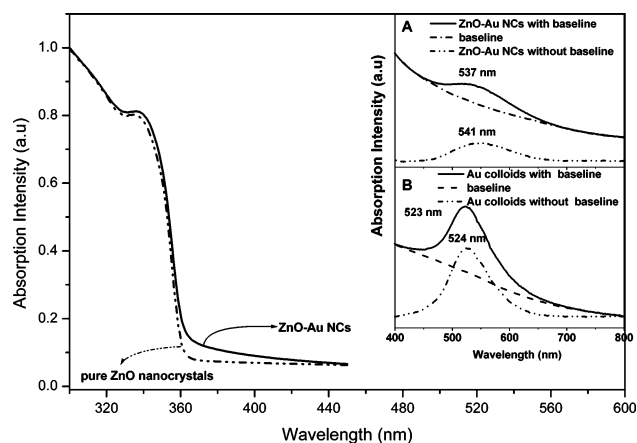

Figure 3. Normalized optical absorption spectra of ZnO−Au NCs (solid line) and pure ZnO nanocrystals (dash dot line). Inset: The surface plasmon absorption band in (A) ZnO−Au NCs and (B) monometallic Au nanoparticles.

due to the incorporation of Au components. In the sample shown in Figure 2A, about 82% of the particles have dumbbell-like structures with Au attached on the ZnO surface. Figure 2B and 2C show typical high-resolution TEM (HRTEM) images of dumbbell-like ZnO−Au NCs, in which the high contrast difference between ZnO and Au is distinguishable because of the higher electron density of metal Au. The distance between two adjacent planes in wurtzite ZnO is determined to be 0.28 nm, corresponding to (100) planes, and that in fcc structured Au is 0.24 nm, resulting from a group of (111) planes. Here, these crystal planes are not parallel to each other, and the angles between them vary from one nanocrystal to the next. These indicate that the epitaxial growth for the formation of ZnO−Au NCs is less obvious, which is similar to the reported result.[22] Note that the average size of Au is 7.1 nm in the NCs, much smaller than that of monometallic Au colloids ranging from 10 to 30 nm prepared by the same citrate reduction method (TEM image is not shown here).

Optical Properties of ZnO−Au NCs. In this study, the optical properties of ZnO−Au NCs were characterized by UV−visible absorption, PL, and Raman scattering spectroscopy, respectively. Figure 3 shows the absorption spectra of the ZnO−Au NCs (solid line) and pure ZnO nanocrystals (dash-dot line). It is well-known that the band-edge absorption of semiconductor in the quantum-confined size regime (≤ 7.0 nm for ZnO) is dependent on the particle size, which was examined in detail by Haase et al.[33] In the range of 300−450 nm, no distinct variation of absorption characteristics of ZnO in the ZnO−Au NCs was found compared with that of pure ZnO nanocrystals, which implies that no apparent growth of ZnO particles occurred
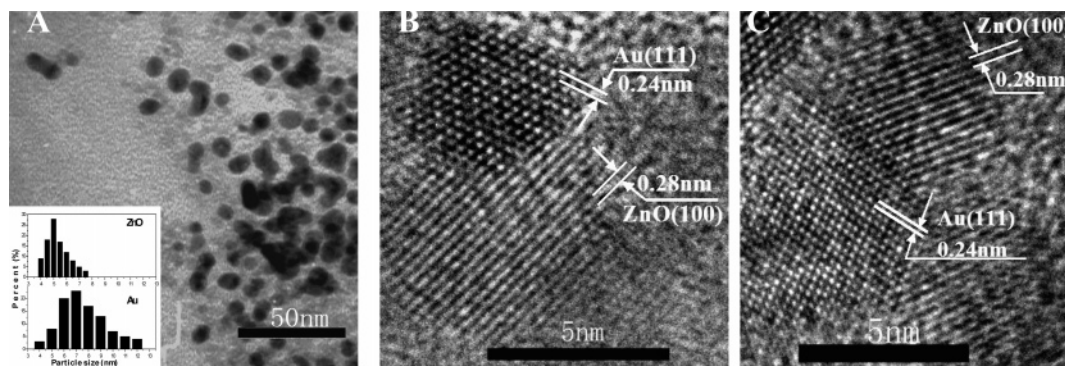

Figure 2. Typical transmission electron microscopy (TEM) image and high-resolution TEM images of ZnO−Au NCs. Inset: Size distribution for ZnO and Au in ZnO NCs, respectively.
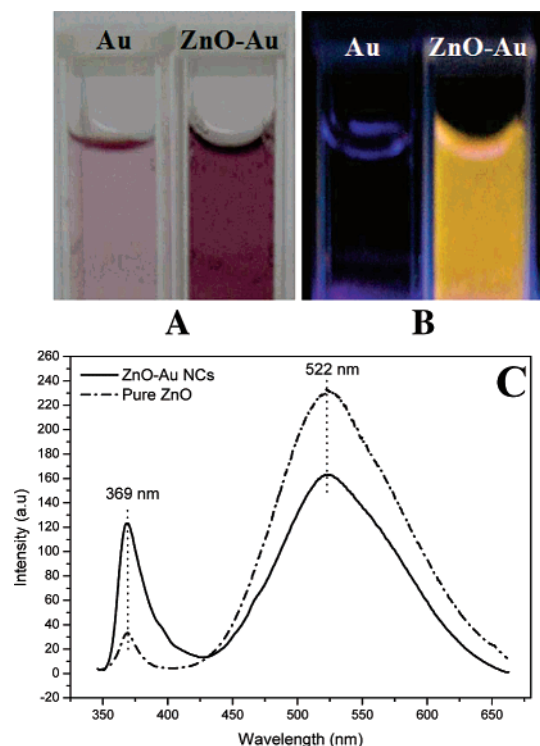
Water-Soluble and Bifunctional ZnO−Au Nanocomposites

J. Phys. Chem. C, Vol. 111, No. 10, 2007 **3839**

Figure 4. Sample photographs of (A) monometallic Au nanoparticles and ZnO−Au NCs in aqueous solution; the corresponding fluorescent images of (B) monometallic Au nanoparticles (no fluorescence) and ZnO−Au NCs in aqueous solution under UV lamp radiation; the photoluminescent spectrum of (C) the ZnO−Au NCs (solid line) and pure ZnO nanocrystals (dash dot line) ($\lambda_{ex} = 340$ nm).

SCHEME 2: The Band Structure of Au and ZnO with Uniform Fermi Level Induced by Electron Transfer between Au and ZnO
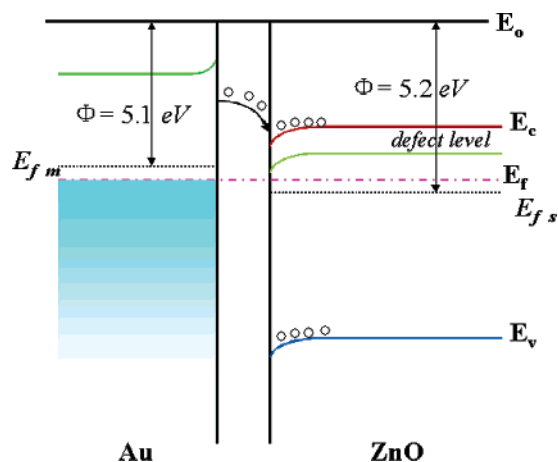
during the formation of the aqueous ZnO−Au NCs. Therefore, the partial aggregation and shape variation shown in the TEM image (Figure 2A) probably comes from the incorporation of Au composition. Furthermore, a surface plasmon band resulting from the noble metal Au in the ZnO−Au NCs as well as a characteristic absorption of ZnO nanocrystals appears in UV−visible spectra. For comparison, monometallic Au nanoparticles (Figure 4A) were also prepared with the same citrate reduction method that produced monometallic Au of 10−30 nm in diameter. The inset of Figure 3 shows the absorption spectra in 400−800 nm for the aqueous solution of ZnO−Au NCs and monometallic Au nanoparticles, respectively. The surface plasmon absorption of citrate-stabilized monometallic Au nanoparticles in water is centered at 524 nm, independent of the
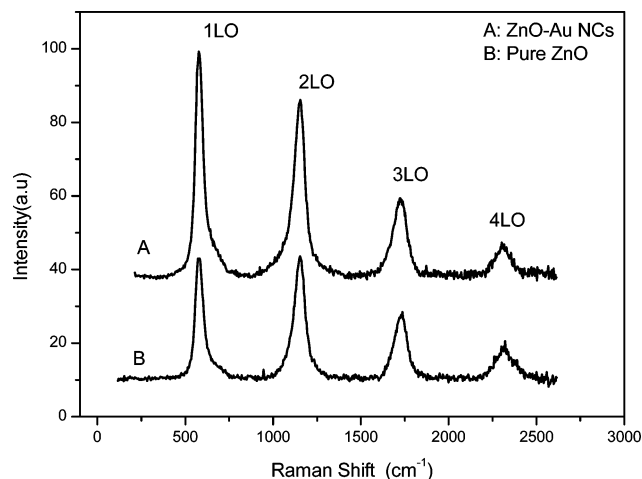

Figure 5. Enhanced multiphonon Raman scattering of (A) ZnO−Au NCs relative to (B) pure ZnO nanocrystals using a He−Cd laser ($\lambda = 325$ nm). The *n* LO refers to the *n*th longitudinal optical phonon.

concentration of the particles. However, absorption of ZnO−Au NCs is not a simple superposition of the characteristic absorptions of ZnO and Au. In fact, the surface plasmon band of ZnO−Au NCs is distinctly broadened and red-shifted by about 17 nm relative to monometallic Au in water medium. It is well-known that the size increase of Au particles causes a red shift of the surface plasmon band.[25] However, the average size of Au here is much smaller in the ZnO−Au NCs than in monometallic Au nanoparticles, which would result in a blue shift instead of the observed red shift if the size effect were responsible. Other factors that might affect the position of the surface plasmon band have also been considered based on the Mie theory, including stabilizing ligands and solvent dielectric, which, however, turned out not to be the primary ones. The change of optical properties was then directed to the strong interfacial coupling between the metal Au and semiconductor ZnO parts in the new heterostructure NCs. Since the Fermi energy level of gold is higher than that of ZnO, a consequence of the fact that the work function is smaller for gold (5.1 eV) than for ZnO (5.2−5.3 eV),[34] electron transfer occurs from Au to ZnO during the formation of ZnO−Au NCs, as shown in Scheme 2, resulting in a uniform Fermi energy level in the ZnO−Au NCs. The transferred electrons subsequently accumulate at the interface of ZnO and Au, causing a downward band bending of the ZnO side. These deficient electrons on the Au surface consequently induce the broadening and red shifting of the surface plasmon band, consistent with previous reports that Au electron deficiency shifts the surface plasmon band to a longer wavelength.[12,16,35,36]

As shown in Figure 4C, the room-temperature PL spectrum of ZnO−Au NCs comprises two emission bands in the UV/visible regions under above band-edge excitation. The corresponding fluorescence image is also given in Figure 4B. The narrow UV emission band centered at 369 nm is assigned to exciton recombination. Despite the intensive studies on the broad visible emission of ZnO, its nature remains controversial; for example, Vanheusder et al. attributed the visible emission to the recombination of holes with the electrons occupying singly ionized oxygen vacancy in ZnO,[37] whereas Dijken et al. ascribed it to the recombination between a deeply trapped hole in a Vo**center and a shallowly trapped electron.[38] Among them, these oxygen vacancies were widely accepted to be responsible for the visible emission of ZnO. It should be noted that the integrated UV emission intensity of ZnO−Au NCs is higher by about 1 order of magnitude than that of pure ZnO nanoc-

rystals. We infer that the enhancement is related to the strong interfacial interaction between ZnO and Au. As mentioned above, the transfer of Au surface electrons to ZnO nanocrystals causes an increase of the Fermi energy level in the ZnO nanocystals, which promotes electron density in the conduction band of ZnO. Moreover, considering that surface plasmon energy of metal Au matches well the emitted visible photon energy of the ZnO nanocrystals, the emitted photons can produce the surface plasmon through energy transfer,[39] which promotes electrons in gold to an excited-state by a surface plasmon wave. The excited electrons will subsequently tunnel into the conduction band of ZnO nanocrystals. Consequently, the increased electron density in the conduction band leads to an increase in the hole−electron recombination rate that enhances the UV emission of ZnO−Au NCs. Accompanying this process, the visible emission in the ZnO−Au NCs is weakened slightly compared with that of the pure ZnO nanocrystals. In addition, the fact that the interfacial interaction between ZnO and Au might lead to charge variation of the Au surface is also the cause of the red shift of the Au surface plasmon band in the ZnO−Au NCs mentioned above.

Resonant Raman spectroscopy can, as a powerful technique, achieve sensitive detection of optical phonon modes and relevant vibration properties. When the excitation energy of 325 nm out of a He−Cd laser is in resonance with the band gap of the wurtzite ZnO, the cross-section of Raman scattering is profoundly enlarged. Therefore, multiphonon scattering is easily observed in the resonant Raman spectra of ZnO−Au NCs and pure ZnO nanocrystals, as shown in Figure 5A and 5B, respectively, where four major sharp bands of longitudinal optical (LO) phonons exist and the frequency shifts are multiples of 1-LO zone-center frequency of 577 cm^{-1}. In the wurtzite structure ZnO with space group C_{6v}, both A_1 and E_1 modes are polar and Raman active. The frequency of the first-order Raman mode at 577 cm^{-1} is between the A_1 (LO) mode (574 cm^{-1}) and the E_1 (LO) mode (591 cm^{-1}), which is a simple sum of both Raman signals. The A_1 (LO) phonon mode at 574 cm^{-1} can only be observed when the *c*-axis is parallel to the sample face, whereas the observation of the E_1 (LO) mode at 591 cm^{-1} is only possible when the *c*-axis is perpendicular to the sample face.[40] The line widths of multiphonon scattering are much greater than that of previously reported single-crystalline bulk ZnO samples and do not follow the relation $\Delta\omega = 9n$ cm^{-1} ($\Delta\omega$ and *n* are the line width and ordinal number of multiphonon scattering, respectively).[41] The observed broadening of phonon lines should probably account for the phonon confinement effect, which has been investigated in detail in the wurtzite ZnO nanocrystals and nanocrystalline silicon.[42−44]

It is interesting to note that the multiphonon scattering is greatly enhanced in the ZnO−Au NCs relative to pure ZnO nanocrystals. As shown in Figure 5A, the enhancement is predominant for the first-order LO phonon mode and then descends with increasing ordinal number of the phonon mode, including the 4LO phonon with slight variation. The 1LO phonon mode of the ZnO−Au NCs shows a 2-fold enhancement compared to that of pure ZnO nanocrystals. Surface-enhanced Raman scattering (SERS) has also been reported in CdS−Ag hybrid particles and CdSe nanobelts (or CdS nanowires) growing epitaxially on the Au (or Ag) surface.[45−46] Theoretical and experimental studies on SERS mechanisms in many cases reveal that the SERS signals are primarily attributed to the electromagnetic excitation of strongly localized surface plasmon of noble metals.[47] In the ZnO−Au NCs, we also count the localized electromagnetic effect of the Au surface plasmon mostly

responsible for the enhancement of multiphonon Raman scattering. In addition, based on the fact that surface plasmon energy of metal Au matches well the emitted visible photon energy from the ZnO nanocrystals, the surface plasmon of the Au nanoparticles might be resonantly excited through energy transfer in the near field and create a stronger local electromagnetic field.[39,48] The incident light field coupling to the local surface plasmon field might induce stronger localized electromagnetic field in the ZnO−Au NCs, which further enhances the multiphonon Raman scattering of ZnO.

Conclusion

The present report demonstrates the chemical synthesis of water-soluble ZnO−Au NCs by a simple and effective route to obtain semiconductor and metal heterostructure composites that are soluble in aqueous media and have expanded functionalities of nanostructured materials. The structures and sizes of ZnO−Au NCs with dumbbell-like shape were identified to be wurtzite ZnO and fcc Au with 4.9 and 7.1 nm diameters, respectively. The surface plasmon band of the ZnO−Au NCs is broadened and red-shifted by about 17 nm relative to monometallic Au nanoparticles. The UV emission of the ZnO−Au NCs is about 1 order of magnitude stronger than that of pure ZnO nanocrystals, which is ascribed to the strong interfacial interactions between ZnO and Au. Furthermore, multiphonon Raman scattering of the ZnO−Au NCs is distinctly enhanced by the strongly localized electromagnetic field of the Au surface plasmon. The water-soluble ZnO−Au NCs with dumbbell-like shape provide a distinct dual functionality: the Au surface can be conjugated, applying well-established Au-thiol chemistry, with thiol-termination or charge-opposite biomolecules, whereas ZnO can be used for fluorescent biolabeling of biomolecules, nanolaser, nanodevices, and efficient catalysts by virtue of its characteristic functional properties.

References and Notes

(1) Colvin, V. L.; Schlamp, M. C.; Alivisators, A. P. *Nature* **1994**, *370*, 354−357.

(2) Artemyev, M. V.; Woggon, U.; Wannemacher, R.; Jaschinski, H.; Langbein, W. *Nano Lett.* **2001**, *1*, 309−314.

(3) Hsu, J. P.; Tian, Z. R.; Simmons, N. C.; Matzke, C. M.; Voigt, J. A.; Liu, J. *Nano Lett.* **2005**, *5*, 83−86.

(4) Alivisatos, A. P. *Science* **1996**, *271*, 933−937.

(5) Bruchez, M.; Moronne, M.; Gin, P.; Weiss, S.; Alivisatos, A. P. *Science* **1998**, *281*, 2013−2015.

(6) Wu, X.; Liu, H.; Liu, J.; Haley, K.; Treadway, J.; Larson, J.; Ge, N.; Peals, F.; Bruchez, M. *Nat. Biotechnol.* **2003**, *21*, 41−46.

(7) Gao, X.; Cui, Y.; Levenson, R. M.; Chung, L.; Nie, S. *Nat. Biotechnol.* **2004**, *22*, 969−976.

(8) Bravner, R.; Ferrari-Iliou, R.; Brivois, N.; Djediat, S.; Benedetti, M. F.; Fievet, F. *Nano Lett.* **2006**, *6*, 866−870.

(9) Pellegrino, T.; Manna, L.; Kudera, S.; Liedl, T.; Koktysh, D.; Rogach, A. L.; Keller, S.; Radler, J.; Natile, G.; Parak, W. J. *Nano Lett.* **2004**, *4*, 703−707.

(10) Larson, D. R.; Zipfel, W. R.; Williams, R. M.; Clark, S. W.; Bruchez, M. P.; Wise, F. W.; Webb, W. W. *Science* **2003**, *300*, 1434−1436.

(11) Daniel, M. C.; Astruc, D. *Chem. Rev.* **2004**, *104*, 293−346.

(12) Cao, Y. W.; Jin, R.; Mirkin, C. A. *J. Am. Chem. Soc.* **2001**, *123*, 7961−7962.

(13) Lyon, J. L.; Fleming, D. A.; Stone, M. B.; Schiffer, P.; Williams, M. E. *Nano. Lett.* **2004**, *4*, 719−723.

Water-Soluble and Bifunctional ZnO−Au Nanocomposites

J. Phys. Chem. C, Vol. 111, No. 10, 2007 **3841**

(14) Cho, S.; Idrobo, J.; Olamit, J.; Liu, K.; Browning, N. K.; Kauzlarich, S. M. *Chem. Mater.* **2005**, *17*, 3181−3186.

(15) Caruntu, D.; Cushing, B. l.; Caruntu, G.; O'Connor, *J. Chem. Mater.* **2005**, *17*, 3398−3402.

(16) Yu, H.; Chen, S.; Rice, P. M.; Wang, S. X.; White, R. L.; Sun, S. *Nano Lett.* **2005**, *5*, 379−382.

(17) Wang, L.; Luo, J.; Fan, Q.; Suzuki, M.; Suzuki, I. S.; Engelhard, M. H.; Lin, Y.; Kim, N.; Wang, J. Q.; Zhong, C. *J. Phys. Chem. B* **2005**, *109*, 21593−21601.

(18) Gu, H.; Yang, Z.; Gao, J.; Chang, C. K.; Xu, B. *J. Am. Chem. Soc.* **2005**, *127*, 34−35.

(19) Mokari, T.; Rothenberg, E.; Popov, I.; Costi, R.; Banin, U. *Science* **2004**, *304*, 1787−1790.

(20) Cumberland, S. L.; Berrettini, M. G.; Javier, A.; Strouse, G. F. *Chem. Mater.* **2003**, *15*, 1047−1056.

(21) Wen, X.; Yang, S. *Nano Lett.* **2002**, *2*, 451−454.

(22) Shi, W.; Sahoo, Y.; Zeng, H.; Ding, Y.; Swihart, M. T.; Prasad, P. N. *Adv. Mater.* **2006**, *18*, 1889−1894.

(23) Spanhel, L.; Anderson, M. A. *J. Am. Chem. Soc.* **1991**, *113*, 2826.

(24) Turkevich, J.; Stevenson, P. L.; Hillier, J. *Discuss. Faraday Soc.* **1951**, *11*, 55.

(25) Petroski, J. M.; Wang, Z. L.; Green, T. C.; El-Sayed, M. A. *J. Phys. Chem. B* **1998**, *102*, 3316.

(26) Comotti, M.; Li, W.; Spliethoff, B.; Schuth, F. *J. Am. Chem. Soc.* **2006**, *128*, 917−924.

(27) Kim, H.; Achermann, M.; Balet, L. P.; Hollingsworth, J. A.; Klimov, V. I. *J. Am. Chem. Soc.* **2005**, *127*, 544−546.

(28) Kwon, K. W.; Shim, M. *J. Am. Chem. Soc.* **2005**, *127*, 10269−10275.

(29) Gu, H.; Zheng, R.; Zhang, X.; Xu, B. *J. Am. Chem. Soc.* **2004**, *126*, 5664−5665.

(30) Westcott, S. L.; Oldenburg, S. J.; Lee, T. R.; Hallas, N. J. *Langmuir* **1998**, *14*, 5396−5401.

(31) Galow, T. H.; Boal, A. K.; Rotello, V. M. *Adv. Mater.* **2000**, *12*, 576−579.

(32) Oldenburg, S. J.; Averitt, R. D.; Westcott, S. L.; Halas, N. *J. Chem. Phys. Lett.* **1998**, *288*, 243−247.

(33) Haase, M.; Weller, H.; Henglein, A. *J. Phys. Chem.* **1988**, *92*, 482−487.

(34) Wang, X.; Summers, C. J.; Wang, Z. L. *Appl. Phys. Lett.* **2005**, *86*, 013111.

(35) Daniel, M. C.; Astruc, D. *Chem. Rev.* **2004**, *104*, 293−346.

(36) Link, S.; El-Sayed, M. A. *Int. Rev. In. Phys. Chem.* **2000**, *19*, 409−453.

(37) Vanheusden, K.; Warren, W. L.; Seager, C. H.; Tallant, D. R.; Voigt, J. A. *J. Appl. Phys.* **1996**, *79*, 7983−7990.

(38) Van Dijken, A.; Meulenkamp, E. A.; Vanmaekelbergh, D.; Meijerink, A. *J. Phys. Chem. B* **2000**, *104*, 1715.

(39) Okamoto, K.; Niki, I.; Shvartser, A.; Narukawa, Y.; Mukai, T.; Scherer, A. *Nat. Mater.* **2004**, *3*, 601−605.

(40) Ashkenov, N.; Mbenkum, B. N.; Bundesmann, C.; Riede, V.; Lorenz, M.; Spemann, D.; Kaidashev, E. M.; Kasic, A.; Schubert, M.; Grendmann, M. *J. Appl. Phys.* **2003**, *93*, 126−133.

(41) Scott, J. F. *Phys. Rev. B* **1970**, *2*, 1209−1211.

(42) Fonoberov, V. A.; Balandin, A. A. *Phys. Rev. B* **2004**, *70*, 233205.

(43) Rajalakshmi, M.; Arora, A. K.; Bendre, B. S.; Mahamuni, S. *J. Appl. Phys.* **2000**, *87*, 2445−2448.

(44) Mishra, P.; Jain, K. P. *Phys. Rev. B* **2001**, *64*, 073304.

(45) Honma, I.; Sano, T.; Komiyama, H. *J. Phys. Chem.* **1993**, *97*, 6692−6695.

(46) Venugopal, R.; Lin, P. I.; Liu, C. C.; Chen, Y. T. *J. Am. Chem. Soc.* **2005**, *127*, 11262−11268.

(47) Garcia-Vidal, F. J.; Pendry, J. B. *Phys. Rev. Lett.* **1996**, *77*, 1163−1166.

(48) Song, J. H.; Atay, T.; Shi, S.; Urabe, H.; Nurmkko, A. V. *Nano Lett.* **2005**, *5*, 1557−1561.